Supplementary Materials for

Rapid carbon mineralization for permanent disposal of anthropogenic carbon dioxide emissions

Matter et al.

Materials and Methods

1) The SF_6 and SF_5CF_3 tracers

SF_6 and SF_5CF_3, originally stored in gas cylinders, were mixed into the CO_2 and CO_2+H_2S flue gas stream using mass flow controllers. Carbon-14 was added to the water injection stream as an aqueous $H^{14}CO_3^-$ solution using a Milton Roy micro-dosing pump (Model AA973-352S3). The $H^{14}CO_3^-$ solution was created by adding 10 mCi of a ^{14}C-rich sodium bicarbonate aqueous solution obtained from Perkin Elmer to 100 liter of groundwater collected from the target storage reservoir prior to CO_2 injection.

Fluid samples for SF_6 and SF_5CF_3 analyses were collected in evacuated 100 ml glass serum bottles from the monitoring well HN04. Concentrations in the headspace were measured with a precision of ±2% using gas chromatography (SRI 8610C) and ultrapure nitrogen as the carrier gas. The headspace samples were injected into a 6ft long, 1/8” wide pre-column with a 5 ångström molecular sieve (MS-5A) and a 6ft chromatographic column at 60°C. SF_6 and SF_5CF_3 concentrations were measured using a SRI 8610C gas chromatograph with an

electron capture detector and a Alltech Carbograph column. Results were recorded using the PeakSimple 3.07.2 software, and concentrations in the water samples were calculated based on the volume of headspace and the solubility.

The SF_6 concentration data from the Phase I injection had to be corrected for the SF_6 that originated from a previous hydrological tracer test. In 2008, we injected SF_6 and sodium fluorescein (Na-Flu) into the target storage reservoir during a short duration tracer test to characterize the hydrology of the injection site. During the Phase I CO_2 injection only SF_6 was injected. Thus, the difference between the observed Na-Flu and the SF_6/Na-Flu ratio can be used to calculate how much SF_6 in the collected water samples is from the Phase I injection (Table S2). Without the addition from the Phase I injection, the SF_6/Na-Flu ratio would follow the trajectory of the Na-Flu concentration. Thus, multiplying the expected ratio by the observed Na-Flu concentration provides a measure of the expected SF_6 concentration. The difference between the observed and expected SF_6 concentration is the actual SF_6 from the Phase I injection (Table S2).

2) Carbon-14

Fluid samples for ^{14}C analysis were collected in 125 ml glass serum bottles. For ^{14}C analysis, water samples were acidified to release the dissolved inorganic carbon as CO_2. The ^{14}C concentration was measured with ^{14}C-AMS first in the W.M. Keck Carbon Cycle Accelerator Mass Spectrometry Laboratory at the University of California, Irvine, and later in the BioAMS laboratory at Lawrence Livermore National Laboratory, USA. Results are reported as fractions of the Modern Standard, $\Delta^{14}C$, following the conventions of Stuiver and Polach (*24*). All results are corrected for isotopic fractionation with $\delta^{13}C$ values measured on prepared samples using AMS spectrometer. Data and uncertainties are reported in Table S2.

3) Dissolved inorganic carbon (DIC)

Dissolved inorganic carbon (DIC) was calculated using PHREEQC (*25*) from measured pH, alkalinity, *in-situ* temperature and total dissolved element concentration measurements. The pH was determined in the field with a Eutech InstrumentsTM CyberScan pH 110 electrode calibrated using NBS standards, and verified in the laboratory a few hours after sampling with a Cole Parmer glass pH electrode. Alkalinity titration was performed using the Gran function to determine the end point of the titration (*26*). The concentration of major elements including Si, Ca, K, Mg, Na, and S and the trace metals Fe and Al were determined by Inductively Coupled Plasma Optical Emission Spectrometry (ICP-OES) using an in-house multi-elements standard checked against the SPEX Certified Reference standard at the University of Iceland. The uncertainties on calculated DIC measurements are estimated to be ±5%

4) Mass balance calculations

Mass balance calculations for dissolved inorganic carbon and ^{14}C were performed to assess the reactivity of the injected CO_2 (27). The mixing fraction between the injected solution (IS) and ambient groundwater (BW) was calculated for each extracted water sample (i) using

$$\left[SF_6\right]_i = X\left[SF_6\right]_{IS} + \left(1-X\right)\left[SF_6\right]_{BW} \quad (1)$$

with *X* being the fraction of injected solution in the extracted water sample. The expected DIC and ^{14}C values due to pure mixing was then determined from

$$DIC_{mix} = X \cdot DIC_{IS} + (1-X) \cdot DIC_{BW} \quad (2)$$

and

$$^{14}C_{mix} = X \cdot {}^{14}C_{IS} + \left(1-X\right) \cdot {}^{14}C_{BW} \quad (3)$$

Differences in DIC and ^{14}C concentrations between the values measured in the retrieved fluid samples and the expected values assuming only mixing between injectate and ambient groundwater yield the loss of DIC and ^{14}C due to carbonate precipitation.

5) Analysis of solid phases

Mineral precipitate samples collected from the submersible pump in monitoring borehole HN04 were analyzed by X-Ray diffraction (XRD), scanning electron microscopy (SEM), and energy dispersive X-ray spectroscopy (EDXS) mapping. Prior to analysis, the samples were stored and treated in an anaerobic chamber to minimize oxidation.

Samples for XRD were mounted on low background Si sample holders and covered with an X-ray transparent cup (Bruker) to decrease oxidation of the fine-grained material during measurement. Measurements were conducted on a Bruker D8 DISCOVER equipped with a LynxEye detector and a Co-source. Scan range was 5-80° using a 0.05° step size and a count time of 10 s per step. Two types of samples were prepared for SEM-EDXS. One set was mounted directly on the Al-sample stubs to avoid a carbon signal from carbon tape. The material was resuspended in anoxic ethanol and a drop of it transferred to the sample holder and left to dry. These samples were imaged by SEM using low vacuum (60 Pa) to minimize sample charging. For another set of samples, the Al-sample holders were covered with carbon tape and grains were picked from the samples and mounted upright to enable imaging of these grains perpendicular to the growth direction. These samples were sputter coated with Au and imaged under high vacuum (4×10^{-4} Pa) to resolved detailed morphological features. SEM/EDXS measurements were conducted on a FEI Quanta 3D FEG SEM equipped with an Oxford instrument X-max 20 mm^2 EDXS detector having a nominal energy resolution of 0.125 keV for Mn$K\alpha$ (FWMH). During imaging, accelerating voltage was 20 KeV and currents were 3.8 pA for SEM imaging and 8 nA for EDXS mapping. In the EDXS maps, color intensity for an element is linearly correlated with the integrated intensity measured in a narrow range round it characteristic X-ray (Ca$K\alpha$: 3.63-3.75 KeV; Fe$K\alpha$: 6.32-6.48 KeV; Si$K\alpha$: 1.69-1.79 KeV; O$K\alpha$: 0.49-0.56 KeV; C$K\alpha$: 0.24-0.29 KeV; peak from C$K\alpha$ has a slight contribution of <5% from Au_N lines).

XRD of all materials from the monitoring borehole (Fig. S1) shows only the Bragg peaks expected for calcite [e.g. (*28, 29*)]. Please note that the broad peaks between 10 and 30° are from the cap protecting the sample from oxidation. SEM imaging and EDXS mapping clearly show 10 um to 1 mm slightly elongated grains rich in Ca, C, and O, as expected for calcite, with trace concentrations of Mg, Mn, and Fe (Fig. S2). Imaging of samples EDXS mapping of the grains collected from inside the pump shows a banded structure where they were fractured, with a first generation of calcite containing rich in Fe- and Si and a second generation largely without such material (Fig. S3).

Laboratory studies of basalt carbonation.

A large number of laboratory experiments have been performed to assess the feasibility of basalt carbonation as a carbon storage strategy (e.g. 15, 16, 30, 31, 32, 33). Such experiments demonstrate the efficient carbonation of basalts and its constituent minerals. During basalt-water-CO_2 interaction, calcium liberated by basalt dissolution tends to provoke calcite precipitation, whereas the liberated magnesium, aluminum and silicon tend to provoke the formation of zeolite and clay minerals (15, 16, 32).

Several experimental studies have been aimed at assessing if precipitated carbonate minerals would eventually slow the overall carbonation rates of basalts and its constituent minerals (9,10). Such studies suggest that the carbonate minerals that precipitate on the surfaces of these rocks and minerals have little effect on the dissolution rates of the original solid and on their carbonation rates. These results were attributed to the poor structural match between the dissolving silicate and precipitating carbonate, which leaves sufficient pathways for chemical mass transfer to and from the adjoining fluid phase (e.g. 34). Such results suggest that the in-situ carbonation of basalts will be little effected by the precipitation of carbonate phases on their surfaces.

In situ fluid chemistry and transport

Representative pre-injection fluid chemistries at the injection site are summarized in Table S2. The temperature gradient at the injection site is 80 °C/km. Groundwater flow in the top tens of meters is to southwest (16); water flow in the lower part of the system is focused in lava flows located at the CO_2 injection depth of 400–800 m depth. The flow rate in this lower system is on the order of 25 m per year and the hydraulic head decreases toward southwest (15, 16). Hydrological models, pump tests and tracer tests, suggest that the effective matrix porosity of this lava formation is 8.5% (16).

The injection of CO_2-charged waters lead to a pH drop in the formation waters provoking the dissolution of basalt and the eventual precipitation of carbonate minerals. In addition to the natural ambient water flow in the target basaltic reservoir, advective transport in the system was enhanced by the continuous pumping of water into the HN-02 injection well and pumping of water from the HN-04 monitoring well at a rate of 1 l/s throughout the study period. The dominance of advection as the chemical transport mechanism in the system is evident in the concentration of chemical tracer in the monitoring fluid shown in Fig. 2; aqueous diffusion is far too slow to transport substantial material from the injection to the monitoring well over the 2-year study period.

Supporting Tables

Table S1. Injection test parameters, including results from the tracer and chemical analysis of injectate.

Injection Phase	CO_2 (tons)	H_2O (liters)	SF_6 (ccSTP/cc)	SF_5CF_3 (ccSTP/cc)	^{14}C (fraction modern)	DIC (mol/L)	pH
I	175	4.8×10^{6}	2.33×10^{-8}	none	16.17	0.82	3.85 (@20°C)
II	54.75	2.25×10^{6}	none	2.24×10^{-8}	4.65	0.43	4.03 (@20°C)

Table S2. Representative water chemistries at the CarbFix injection site prior to the gas injections (after 15).

	Well		
Parameter or aqueous concentration	HN-1 (source of injection water)	HN-2	HN-4
Sample	08HAA02	09HAA16	08HAA01
Sampling date	1 July 2008	19 May 2009	1 July 2008
Temperature °C	19.0	15.5	32.3
pH at 20 ±2 °C	8.87	8.79	9.43
O_2 (mmol/L)	0.057	0.011	0.037
Alkalinity (meq/kg)	1.91	1.45	1.91
F (mmol/L)	0.014	0.013	0.026
Cl (mm/L)	0.247	0.222	0.228
SO_4 (mmol/L)	0.075	0.077	0.089
Na (mmol/L)	1.301	1.338	2.114
K (mmol/L)	0.027	0.012	0.019
Ca (mmol/L)	0.164	0.124	0.041
Mg (mmol/L)	0.313	0.149	0.005
Fe (µmol/)	0.016	0.399	0.064
Al (µmol/)	0.419	0.097	1.905
Si (mmol/L)	0.363	0.337	0.897

Table S3: Result from the tracer and chemical fluid analyses.

Sample ID	Days since injection started	Na-Flu (g/L)	SF_6 (ccSTP/cc)	SF_6 Phase I (ccSTP/cc)*	SF_5CF_3 Phase II (ccSTP/cc)	pH	DIC (mmol/ L)	^{14}C (frac. modern)	±	^{14}C (Bq/L)
619	1	4.94E-05	1.51E-09	2.44E-12		9.24	1.54			
621	2		1.54E-09							
623	3	4.98E-05	1.45E-09			9.32	1.5			
629	6	5.05E-05	1.62E-09	4.34E-11		9.38	1.47	0.3119	0.0008	0.001377
643	13	5.15E-05	1.56E-09			9.27	1.54	1.328	0.002	0.006584
651	16	5.15E-05	2.09E-09	4.52E-10		8.98	1.87			
655	18		1.90E-09							
661	21	5.14E-05	1.70E-09	6.58E-11		8.86	2.01	3.5054	0.0049	0.02117
665	23		2.02E-09			7.94	2.32			
667	24	5.14E-05	2.10E-09	4.70E-10		7.46	2.53			
669	25	5.14E-05	2.41E-09	7.75E-10		7.27	2.63	8.4908	0.0119	0.06685
679	31	5.23E-05	3.18E-09	1.48E-09		6.93	3.18			
681	32		3.25E-09			7.18	2.85			
687	35	5.36E-05	3.09E-09	1.31E-09		6.98	2.97	9.0563	0.0217	0.08001
693	38	5.43E-05	3.35E-09	1.52E-09		6.91	3.26	10.8941	0.0516	0.10575
699	42	5.54E-05	3.26E-09	1.36E-09		6.81	3.6	9.8633	0.0338	0.09663
703	44	5.46E-05	3.16E-09	1.31E-09		6.79	3.63	9.2766	0.0647	0.08921
705	48	5.00E-05	3.52E-09	1.97E-09		6.63	4.1	9.1683	0.0641	0.09506
709	49		3.70E-09							
715	51	4.92E-05	3.27E-09	1.78E-09		6.57	4.39	9.908	0.0758	0.10749
721	56	4.90E-05	4.05E-09	2.57E-09		6.64	4.18	10.9666	0.0696	0.11732
723	59	4.90E-05	3.34E-09	1.86E-09		6.68	4.03			
733	64	4.88E-05	4.24E-09	2.78E-09		6.81	3.65	11.1269	0.0637	0.10968
741	71	4.86E-05	3.36E-09	1.91E-09		7.06	3.19	10.3135	0.0805	0.09608
747	78	4.85E-05	3.47E-09	2.03E-09		7.22	3.07	10.963	0.089	0.09488
753	84	4.83E-05	2.99E-09	1.55E-09		7.63	2.74	10.963	0.089	0.09488
763	92	5.03E-05	3.21E-09	1.65E-09		7.92	2.61	11.2236	0.1119	0.08778
775	111	5.51E-05	3.28E-09	1.40E-09		8.65	2.32	9.0533	0.052	0.06502
777	115	4.96E-05	2.81E-09	1.30E-09		8.92	2.15			
781	118	4.90E-05	2.56E-09	1.08E-09		8.92	2.31			
783	122	4.85E-05	3.12E-09	1.67E-09		8.76	2.22	8.0588	0.0616	0.05473
785	127	4.74E-05	3.04E-09	1.66E-09		8.81	2.24			
787	129	4.70E-05	3.52E-09	2.16E-09		8.76	2.22			
789	136	4.57E-05	3.49E-09	2.21E-09		8.82	2.27	8.6288	0.0795	0.05938
793	139	4.50E-05	3.41E-09	2.17E-09		8.78	2.3			
797	147	4.29E-05	3.53E-09	2.41E-09		8.68	2.43			
801	148	4.29E-05	4.42E-09	3.30E-09		8.62	2.5	8.4219	0.0742	0.06251
803	149		4.04E-09							
813	156	4.16E-05	4.22E-09	3.17E-09	2.66E-11	7.36	3	8.0027	0.0593	0.06998

819	161	4.18E-05	4.15E-09	3.09E-09	2.18E-11	8.11	2.55			
825	164		4.19E-09		1.99E-11	8.43	2.66			
831	168	4.00E-05	4.37E-09	3.40E-09	2.35E-11	8.36	2.57	8.4363	0.0521	0.06516
833	169	3.90E-05	4.37E-09	3.45E-09	2.14E-11	8.33	2.55			
841	183	3.78E-05	4.50E-09	3.64E-09	3.09E-11	7.87	2.75	7.769	0.0512	0.0628
847	204	3.64E-05	5.43E-09	4.64E-09	4.09E-11	7.07	3.31			
849	213	3.60E-05	5.78E-09	5.01E-09	3.49E-11	7.50	2.98			
850	218	3.56E-05	5.81E-09	5.06E-09	2.75E-11	7.93	2.82			
851	225	3.51E-05	6.23E-09	5.50E-09	2.65E-11	8.19	2.77			
853	234	3.42E-05	6.87E-09	6.17E-09	2.36E-11	7.56	2.84	7.9298	0.0512	0.06267
855	245	3.37E-05	6.90E-09	6.22E-09	2.01E-11	8.29	2.66			
857	252	3.34E-05	7.42E-09	6.76E-09	2.35E-11	8.30	2.64			
858	259	3.34E-05	7.84E-09	7.18E-09	2.08E-11	8.36	2.57			
859	266	3.26E-05	7.94E-09	7.32E-09	2.20E-11			7.4848	0.0776	0.06051
860	273	3.21E-05	7.69E-09	7.08E-09	1.95E-11	8.40	2.59			
861	280	3.09E-05	8.42E-09	7.86E-09	2.45E-11	8.26	2.63			
863	296	3.00E-05	8.92E-09	8.39E-09	2.46E-11	8.31	2.61	8.4791	0.0742	0.06498
865	308	2.94E-05	9.09E-09	8.58E-09	2.42E-11	8.30	2.61			
869	322	2.92E-05	9.15E-09	8.66E-09	2.35E-11	8.31	2.51	8.3668	0.0657	0.06009
873	332	2.88E-05	9.65E-09	9.17E-09	2.56E-11	8.41	2.45			
875	350	2.88E-05	9.79E-09	9.31E-09	2.96E-11	8.73	2.37			
877	367	2.69E-05	1.03E-08	9.88E-09	3.77E-11	8.58	2.68			
879	386	2.47E-05	9.72E-09	9.37E-09	4.88E-11	8.57	2.67			
881	406	2.31E-05	1.10E-08	1.07E-08	5.81E-11	8.20	2.83			
883	423	2.33E-05	9.94E-09	9.63E-09	5.65E-11	8.45	2.54			
881	436	2.26E-05	9.03E-09	8.75E-09	4.87E-11	8.76	2.39			
889	444	2.15E-05	8.77E-09	8.52E-09	6.30E-11	8.93	2.4			
893	449	2.17E-05	8.93E-09	8.67E-09	5.92E-11	8.76	2.43			
895	454	2.15E-05	8.65E-09	8.40E-09	5.52E-11					
897	470	2.13E-05	8.07E-09	7.82E-09	5.76E-11	8.81	2.35			
901	477	2.09E-05	8.90E-09	8.66E-09		8.91	2.32			
905	484	2.05E-05	8.93E-09	8.70E-09		8.95	2.28			
907	491	1.92E-05	7.07E-09	6.87E-09		8.94	2.41	7.5505	0.0467	0.05559
909	498	1.92E-05	9.10E-09	8.91E-09		8.94	2.34			
913	511	2.20E-05	9.57E-09	9.30E-09	7.26E-11	8.83	2.33	6.5517	0.0472	0.04745
915	518		8.28E-09		6.61E-11	8.83	2.27	6.2029		0.04231
917	525		9.80E-09		7.59E-11	8.93	2.34	7.2165		0.05075
918	539		9.39E-09		6.96E-11	8.99	2.23	6.6135		0.04571

Supporting Figures

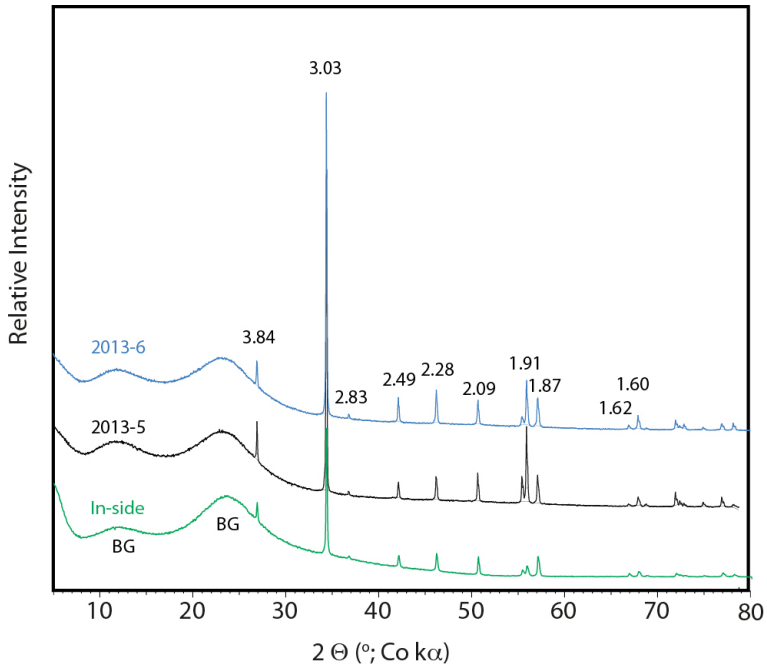

Figure S1. X-ray tracers of sample 2013-5 and 2013-6 taken from the submersible pump. The two broad peaks are from the cap protecting the sample from further oxidation is marked BG.

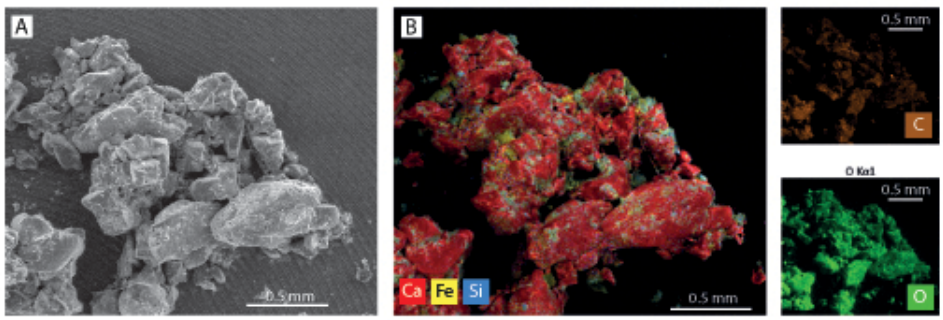

Figure S2. Overview SEM images and EDX maps of material from sample 2013-6. (**A**) SEM image. (**B**) EDX map of are shown in SEM image A. The maps for Ca, Fe and Si has been overlain the SEM image, whereas the maps for C and O are presented individually.

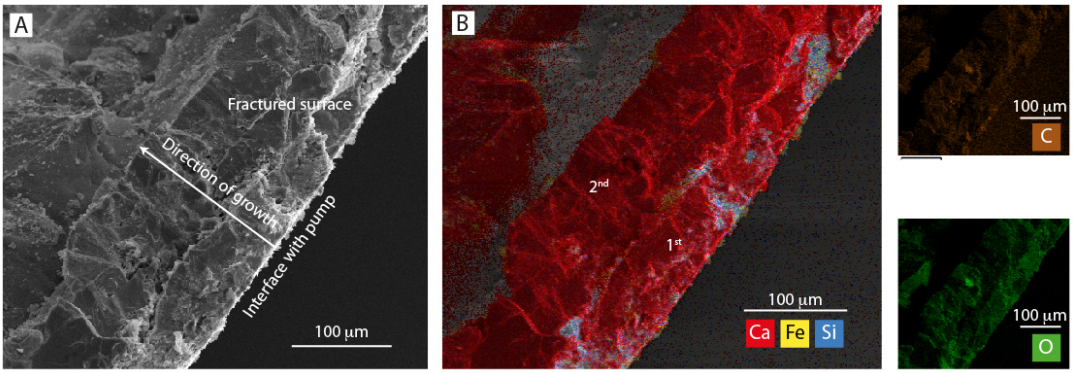

Figure S3. SEM images and EDX maps of fractured flake from a sample collected inside the submersible pump. (**A**) SEM image of the fractured flake mounted upright so that the internal regions of the material could be imaged. Fractured region, where the material interfaced with the pump surface and the direction of mineral growth is indicated. (**B**) EDX maps of area shown in SEM image A. The maps for Ca, Fe and Si has been overlain the SEM image, whereas the maps for C and O are presented individually. The location of two generations of calcite have been indicated based on the frequency of Fe- and Si-rich material.